PHYSICS AND CHEMISTRY OF SOLID STATE
V. 24, No. 2 (2023) pp. 235-243
Section: Chemistry

DOI: 10.15330/pcss.24.2.235-243

Vasyl Stefanyk Precarpathian National University

ФІЗИКА І ХІМІЯ ТВЕРДОГО ТІЛА
Т. 24, № 2 (2023) С. 235-243
Хімічні науки

PACS: 61.66.Fn ISSN 1729-4428

Oleksandr Smitiukh[1], Oksana Soroka[2], and Oleg Marchuk[1]

Effect of the crystal structure and chemical bonding on the electronic and thermal transport in $Cu_2MeHf_3S_8$ (Me – Mn, Fe, Co, Ni) thiospinels

[1]*Department of Chemistry, Ecology and Pharmacy,Lesya Ukrainka Volyn National University, Lutsk, Ukraine, Smitiukh.Oleksandr@vnu.edu.ua*
[2]*Ivano-Frankivsk National Medical University, Ivano-Frankivsk, Ukraine*

Establishing the relationship between crystal structure and transport properties is an important issue that is directly connected with the applicability of functional materials. In this work, we present the analysis of the crystal structure, chemical bonding, and electronic and thermal transport properties of $Cu_2MeHf_3S_8$ (*Me* – Mn, Fe, Co, Ni) compounds. The increase of weighted mobility in the Mn → Fe → Co → Ni series as well as the change of the dominant scattering mechanism of charge carriers from scattering on point defects to the scattering on acoustic phonons explains the best electronic transport in $Cu_2NiHf_3S_8$. Moreover, bonding inhomogeneity between the covalent δ(Co – S) and δ(Hf – S) from one side, and more ionic δ(Cu – S) interactions from the other side leads to low lattice thermal conductivity in $Cu_2MeHf_3S_8$ (*Me* – Mn, Fe, Co, Ni) materials. The work also suggests the link between the occupation of the octahedral 16*d* site and the thermoelectric performance of the investigated thiospinels. Particularly, the best thermoelectric performance is observed in the case of the presence of two valence electrons in the *d*-level of atoms in octahedral voids, which can be essential for further enhancement of the thermoelectric performance in thiospinels.

Keywords: bonding inhomogeneity; crystal structure; weighted mobility; thermal conductivity; quaternary sulfides.

Received 30 August 2022; Accepted 24 March 2023.

Introduction

Development of the new materials with ultralow thermal conductivity for thermoelectrics and thermal barrier coatings is among the hot topics in modern materials science [1–4]. However, materials with low thermal conductivity usually contain heavy and hazardous elements [5–8], which is in contradiction with the required low weight of thermoelectric devices [9,10] and even more crucial for the thermal barrier coatings used for the protection of aircraft turbines [4]. However, a lot of recent works show that ultralow thermal conductivity can be achieved even in materials consisting of lightweight elements through the crystal structure complexity engineering and chemical bonding hierarchy [3,11–15]. Among the most successful approaches for the reduction of lattice thermal conductivity are the phonon-liquid electron-crystal (PLEC) concept (which is based on the liquid-like behavior of superionic conductors) [2,12,13,16], bonding anisotropy in layered structures [8,17,18], lattice anharmonicity induced by the lone-pair-electrons [5,19–21] and bonding inhomogeneity [22–24]. Following the market requirements, sulfides attract more attention recently and they are frequent objects of current investigations [25–28].

A lot of promising environmental-friendly sulfides with low thermal conductivity were explored recently. Among them, special attention was devoted to the binary copper-based sulfides $Cu_{2-x}S$ [29], chalcopyrites [30,31], ternary Cu-Sn-S semiconductors [32,33], colusites [34], tetrahedrites [13,35], argyrodites [12,36], and some others [37]. However, often low thermal conductivity in these

compounds is caused by weak chemical bonding which in turn leads to the low thermal stability of the majority of these compounds (e.g. $Cu_{2-x}S$, Cu-rich tetrahedrites, and argyrodites) [2]. This reason restricts the wide utilization of such materials for energy converters and thermal barrier coatings due to the structural degradation of the materials at elevated temperatures [38,39]. Therefore, the effective compromise between disturbed phonon transport and the thermal stability of materials is still a great challenge. Ternary and quaternary transition metal thiospinels are the perspective materials that can effectively meet both requirements [40,41].

The phases based on the $MgAl_2O_4$ crystal structure type attract special attention. The structure of spinels with the general formula AB_2X_4 is based on the diamond structure. The 8*a* site of *A* atoms corresponds to the diamond structure, *B* atoms occupy the 16*d* site, and X atoms are in the 32*e* site. The unit cell of the AB_2X_4 structures can be expressed as $A_8B_{16}X_{32}$. The cations occupy one-eighth of the tetrahedral sites and half of the octahedral sites. Such a structure favors the low thermal conductivity in the $Cu_2MeHf_3S_8$ materials (*Me* = Mn, Fe, Co, Ni) [9]. However, the finding of the correlation between the crystal structure and the transport properties of the spinel structure is an important task.

Aiming to find stable materials with low thermal conductivity, this study is dedicated to the investigation of the relations between the crystal structure of $Cu_2MeHf_3S_8$ and electronic and thermal transport properties. With this goal, we performed the analysis of structural parameters, chemical bonding, charge carrier mobility, and lattice thermal conductivity. The effective engineering of carrier mobility is crucial for designing electronic devices, while low thermal conductivity is necessary for efficient energy converters and thermal barrier coatings.

I. Experimental details

The concentration tetrahedron of the sulfide systems Cu – *Me* – Hf – S (*Me* – Mn, Fe, Co, Ni) is presented in Fig. 1.

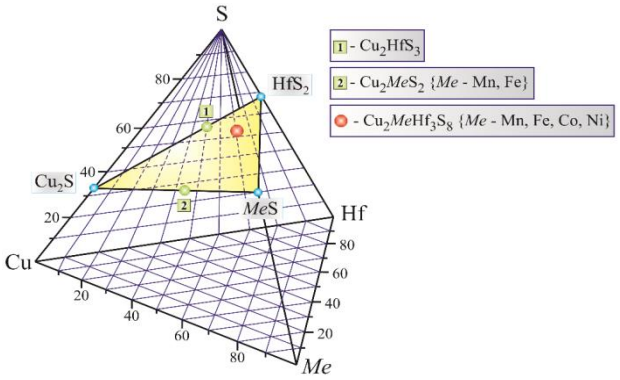

Fig. 1. Quaternary diagram Cu – *Me* – Hf – S and the quasi-ternary section Cu_2S – *Me*S – HfS_2 (*Me* – Mn. Fe, Co, Ni).

The quaternary sulfides $Cu_2MeHf_3S_8$ are formed in the quasi-ternary systems Cu_2S – *Me*S – HfS_2 that are one of the possible sections of the concentration tetrahedron. The $Cu_2MeHf_3S_8$ sulfides can be obtained by various techniques:

a) synthesis from the elementary substances Cu, Mn, Fe, Co, Ni, Hf and S;

b) interaction of the binary sulfides Cu_2S, *Me*S (*Me* – Mn, Fe, Co, Ni) and HfS_2 taken in the ratio of 1:1:3;

c) the $Cu_2MnHf_3S_8$ and $Cu_2FeHf_3S_8$ sulfides can be synthesized from the Cu_2MeS_2 (*Me* – Mn, Fe) and HfS_2 sulfides taken in the ratio of 1:3.

In the present work, we obtained the samples for investigation from high-purity elements. The total mass of a sample was 3g. Co-melting of the elements was held in evacuated ampoules (residual pressure 10^{-2} Pa) in an MP-30 programmable electric muffle furnace in two stages. The first stage was heating to 1423 K (heating rate 12 K/h); exposure to 1423 K for 4 h; cooling to room temperature (cooling rate 12 K/h). At the second stage to obtain homogeneous samples, pre-synthesized ingots were ground into powder and pressed into tablets. These were again placed in evacuated containers, reheated to 773 K at the rate of 12 K/h, annealed at this temperature for 500 h, and quenched into room-temperature water (without depressurizing the containers).

Phase identification was performed with a BRUKER D8 Advance X-ray diffractometer using Cu*K*α-radiation (λ = 1.5418 Å, $\Delta 2\Theta$ = 0.005°, 2Θ range 10 – 120°) with Bragg-Brentano geometry. Rietveld refinement of the crystal structure was performed in the WinCSD program package [42]. Visualization of the crystal structure utilized VESTA program [43].

Quantum chemical (QC) calculations were performed using the Firefly QC program package [44], which is based on the GAMESS (US) source code [45]. The calculations were performed based on the hybrid functional B3LYP that used the Becke GGA functional for the exchange energy, and the Lee-Yang-Parr GGA functional for the correlation energy [46,47]. For the calculations, we employed lattice parameters, symmetry information, and atomic coordinates obtained during the crystal structure refinement of the $Cu_2CoHf_3S_8$ and using literature data for $CuCo_2S_4$ and $CuHf_2S_4$ compounds. The basis sets for the self-consistent calculations can be obtained from the authors. The analysis of the chemical bonding for the investigated materials was performed by the electron localization function. For this purpose, the electron localization function (ELF) maps were calculated and visualized using the specialized module implemented in ChemCraft [48] and Vesta [43] software.

II. Results and discussion

2.1. Chemical bonding analysis in the $Cu_2MeHf_3S_8$ (*Me* – Mn, Fe, Co, Ni) sulfides

Multicomponent chalcogenides are interesting objects from the point of view of the nature of chemical bonding. To a large extent, the nature of the bond is determined by the features of the crystal structure. It is known that the spinel structure can be represented as a stacking of face-centered unit cells in which sulfur atoms form a three-layer closest packing of the ABCABC type (Fig. 2).

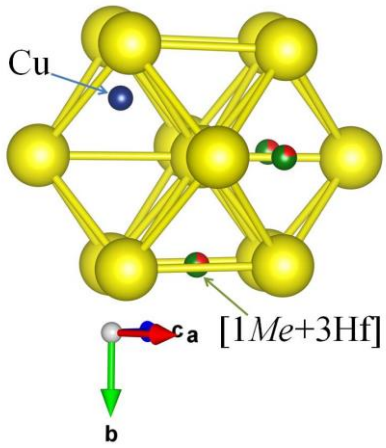

Fig. 2. Closest-packed structure of $Cu_2MeHf_3S_8$ (*Me*–Mn, Fe, Co, Ni) compounds.

To consider the nature of chemical bonding in the $Cu_2MeHf_3S_8$ (*Me* – Mn, Fe, Co, Ni) structure, we employed the data on atomic and ionic radii (Table 1). From the results of the calculation of experimental diffraction patterns, it can be seen that the Cu – S bond has mostly covalent component, with the bond ionicity increasing in the Mn → Fe → Co → Ni series of the $Cu_2MeHf_3S_8$ compounds. The opposite situation is observed for the Hf – S bonds where the covalent component increases in this series. For the *Me* – S bond, the ionicity fraction increases in the Mn → Fe → Co → Ni series. Considering the above analysis, an important role in the structure plays the *Me* metal atoms, which cause the strengthening of the ionic component. If we consider the formation of these phases from the point of view of a three-component system, it is appropriate to compare the values of interatomic distances (Table 2) of the experimentally obtained starting phases Cu_2S, HfS_2, MnS, FeS, CoS, and NiS (Table 3). Hence, in binary compounds, the covalent component prevails.

The crystal structure of the quaternary phases $Cu_2MeHf_3S_8$ (*Me* – Mn, Fe, Co, Ni) has cubic symmetry. The calculated and experimental diffractograms of the compounds are presented in Fig.3. Having the crystal structure with high symmetry of the structural elements, it is simplier to find the relationship between crystal structure and properties because each elements (atomic site, plane etc.) is responsible for appropriate properties

The lattice parameter *a* changes substantially in the Mn→Fe transition. The stable d^5-state in which all electrons of the *d*-sublevel are valence electrons transforms to d^6-state with 4 valence electrons with subsequent reduction of valence electrons (Co–d^7, Ni–d^8). Thus, Ni atoms have only two valence electrons. Hf atoms also have a d^2-state (two-valence electron state).

Table 1.

Data for analysis of the nature of chemical bonds

	Electron configuration of atoms	**r^*_{cov}, Å**	**r^*_{metal}, Å**	**r^*_{ion}, Å**	**Electron configuration of ions**	**r(Me) + r(S)**	**$r(Me^{+x})+ r(S^{2-})$**
Cu	$[Ar]3d^{10}4s^1$	1.17	1.28	0.98 (Cu^{+1})	$[Ar]3d^{10}4s^0$	2.19	2.8
Mn	$[Ar]3d^5 4s^2$	1.17	1.30	0.91 (Mn^{+2})	$[Ar]3d^3 4s^2$	2.19	2.73
Fe	$[Ar]3d^6 4s^2$	1.17	1.26	0.80 (Fe^{+2})	$[Ar]3d^4 4s^2$	2.19	2.62
Co	$[Ar]3d^7 4s^2$	1.16	1.25	0.78 (Co^{+2})	$[Ar]3d^5 4s^2$	2.18	2.6
Ni	$[Ar]3d^8 4s^2$	1.15	1.24	0.74 (Ni^{+2})	$[Ar]3d^6 4s^2$	2.17	2.56
Hf	$[Xe]4f^{14}5d^2 6s^2$	1.44	1.59	0.82 (Hf^{+4})	$[Xe]4f^{14}5d^0 6s^2$	2.46	2.64
S	$[Ne]3s^2 3p^4$	1.02	–	1.82 (S^{-2})	$[Ne]3s^2 3p^6$	–	–

**- Bokiy G. B. Kristallokhimiya. Izd. Tretye. pererabotannoye i dopolnennoye. izdalstvo «Nauka». 1971 g.. str. 400*

Table 2.

Interatomic distances in the $Cu_2MeHf_3S_8$ (*Me* – Mn, Fe, Co, Ni) structure

Bond	**$\delta(Me - X)_{exp}$, Å**			
	$Cu_2MnHf_3S_8$	**$Cu_2FeHf_3S_8$**	**$Cu_2CoHf_3S_8$**	**$Cu_2NiHf_3S_8$**
Cu – S	2.302	2.318	2.334	2.344
Hf – S	2.571	2.538	2.524	2.511
Mn – S	2.571			
Fe – S		2.538		
Co – S			2.524	
Ni – S				2.511

Table 3.

Interatomic distances Me – S

Compound	**Bond**	**$\delta(Me - X)_{exp}$, Å**
Cu_2S (*Fm*–3*m*)	Cu – S	2.3155
HfS_2 (*P*6$_3$/mmc)	Hf – S	2.51278
MnS (*P*6$_3$/mmc)	Mn – S	2.4264
FeS (*P*6$_3$/mmc)	Fe – S	2.4529
CoS (*P*6$_3$/mmc)	Co – S	2.3412
NiS (*P*6$_3$/mmc)	Ni – S	2.3779

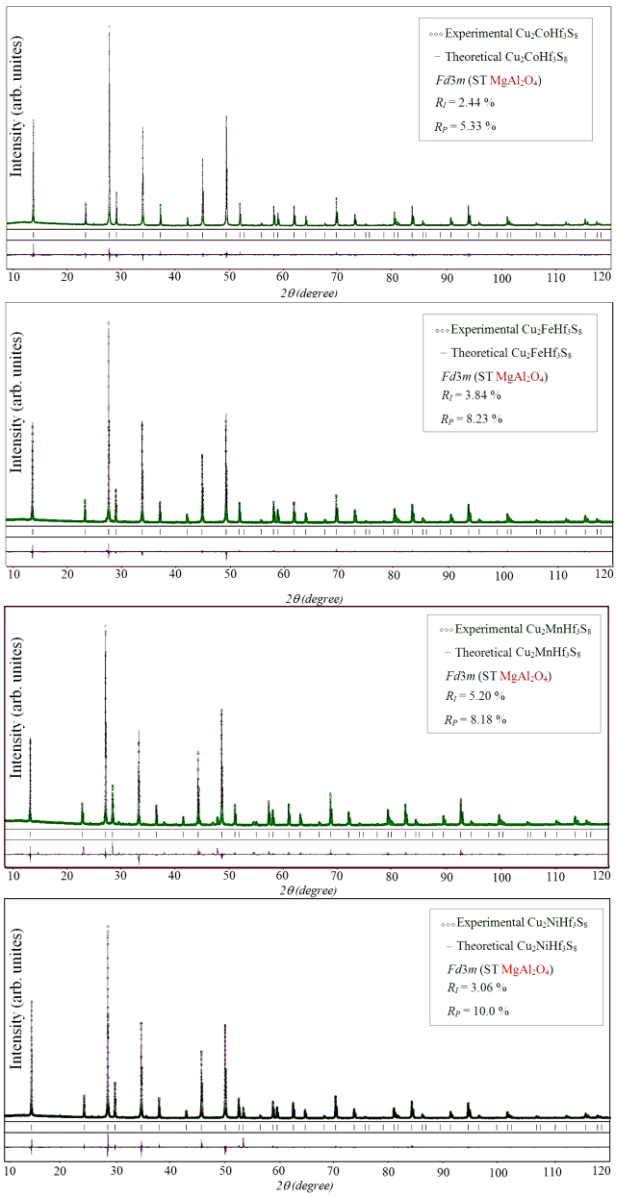

Fig.3. The calculated and experimental diffractograms of $Cu_2MeHf_3S_8$ (*Me* – Mn, Fe, Co, Ni) compounds.

Accordingly, the filling of the 16*d* site with Hf and Ni atoms contributes to the reduction of the thermal conductivity of $Cu_2MeHf_3S_8$ thiospinels. The change of lattice parameters, interatomic distances, atomic coordinates, and bond angles of the compounds are presented in Fig.4(a)(b).

The interatomic distances δ(*Me*/Hf – S) decrease with the decrease of *Me* atomic radii, whereas the δ(Cu–S) distance increases which indicates increasing bond ionicity. The arrangement of atoms in this structure indicates that the change in the 32*e* site coordinates should be considered since the first coordination environment for this site consists of (*Me*/Hf) and Cu atoms. The analysis of graphical dependence (Fig. 4(b)) indicates that the 32*e* site shifts in the direction of the 16*d* site in which the *Me*/Hf statistical mixture is located. Moreover, the Cu – S – (*Me*/Hf) angle decreases in the Mn → Fe → Co → Ni series, and the decrease is almost linear. At the same time, the value of the (*Me*/Hf) – S – (*Me*/Hf) angles increases linearly in the Mn → Fe → Co series, stabilizing at 90° for $Cu_2NiHf_3S_8$.

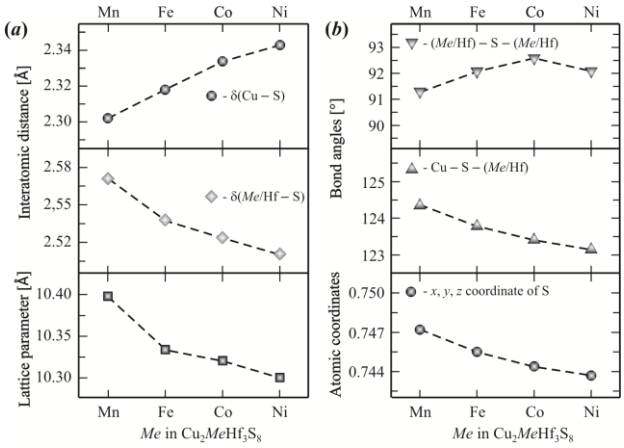

Fig.4. The change of lattice parameter and interatomic distances (a), atomic coordinates and bond angles (b) of $Cu_2MeHf_3S_8$ (*Me* – Mn, Fe, Co, Ni).

The nature of the change in isovalent parameters of atoms is ambiguous. This can be ascertained by analyzing the dependence of thermal oscillations of atoms on the qualitative composition of the studied sulfides (Fig. 5). It can be concluded from the presented dependences that the largest oscillations are shown by copper atoms. It is worth noting that the respective B_{iso} value is stabilized at 1.03 Å^2 in the $Cu_2NiHf_3S_8$ structure. Expectedly, the lowest B_{iso} value is for heavy Hf atoms. The value of the isovalent parameter of S atoms has a tendency to increase in the structure of $Cu_2MnHf_3S_8$, $Cu_2FeHf_3S_8$, and $Cu_2CoHf_3S_8$ while this parameter is decreasing to 0.70 Å^2 in the $Cu_2NiHf_3S_8$ structure. Clearly, copper atoms will have the largest effect on weighted mobility.

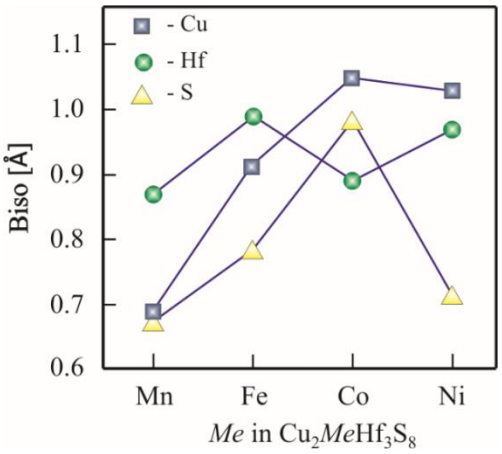

Fig. 5. Dependence of isovalent atomic parameter on composition.

The weighted mobility of state-of-the-art thermoelectric materials decreases with temperature as $T^{-3/2}$ because the electrons are scattered by phonons [49]. To calculate the weighted mobility for $Cu_2MeHf_3S_8$ samples, we used numerical data of temperature-dependent Seebeck coefficient and electrical conductivity from our previous work [9]. The change of weighted mobility of the $Cu_2MeHf_3S_8$ phases (Fig. 6(a)) shows that the increase of mobility with temperature indicates, that the carrier scattering on defects (ionized impurities or grain boundaries) is dominating [49]. The low mobility

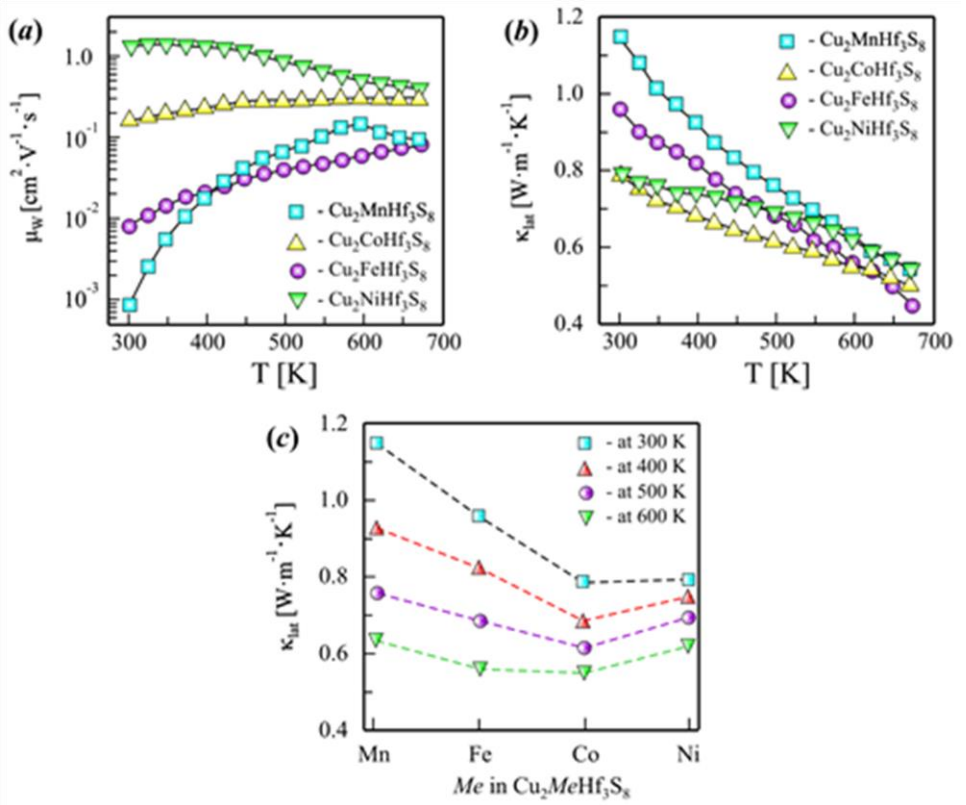

Fig.6. The properties of $Cu_2MeHf_3S_8$ (*Me* – Mn, Fe, Co, Ni): a) weighted mobility, b) thermal conductivity, and (c) the composition and thermal conductivity at 300, 400, 500, and 600 K.

below room temperature could be a sign of grain boundary scattering. However, in contrast with $Cu_2MeHf_3S_8$ (*Me* – Mn, Fe, Co) phases, $Cu_2NiHf_3S_8$ shows decreasing tendency of weighted mobility above 400 K, suggesting that electrons are mainly scattered by phonons as in the state-of-the-art thermoelectric materials [50]. Such a tendency of weighted mobility together with its highest values in the series indicates the best electronic transport in $Cu_2NiHf_3S_8$.

Fig. 6(b) shows the lattice thermal conductivity (κ_{lat}) of the studied $Cu_2MeHf_3S_8$ samples after sintering. All specimens possess very low thermal conductivities, in the range of 0.7–1.2 W m^{-1} K^{-1} at 300 K, decreasing to 0.4–0.7 W m^{-1} K^{-1} at 673 K which are among the lowest values observed in spinel-type materials. Fig. 6(c) shows the compositional dependence of lattice thermal conductivity at selected temperatures for $Cu_2MeHf_3S_8$. The values of κ_{lat} decrease in series Mn → Fe → Co and slightly increase for the Ni-contained sample.

Interestingly, such a compositional dependence of lattice thermal conductivity reflects well the deviations in bond angles and atomic coordinates from its ideal values, as it is shown in Fig. 4(b). This observation suggests a very strong interconnection between the crystal structure distortion and lattice thermal conductivity in the investigated materials. For the deeper analysis of electronic and thermal transport in $Cu_2MeHf_3S_8$ materials and their structural origin, we performed the analysis of chemical bonding between atoms in studied thiospinels.

We decided to start the analysis of chemical bonding from the ternary thiospinels $CuCo_2S_4$ and $CuHf_2S_4$. In the $CuCo_2S_4$ structure, the overlapping of electron clouds between Cu-S atoms is weaker than for Co-S, suggesting a more covalent nature of Co-S bonds. However, in the case of $CuHf_2S_4$, the overlapping of electron clouds between different cations and anions is very similar, suggesting small bonding inhomogeneity. To understand the chemical bonding environment in $Cu_2MeHf_3S_8$ (*Me* – Mn, Fe, Co, Ni), we calculated the electron localization function (ELF). The visualized 3D maps of the ELF sliced on the planes [1 0 1] and [1 0 -1] are shown in Fig. 7.

In order to calculate the electron localization function (ELF) maps for disordered $Cu_2CoHf_3S_8$ with the statistical occupation of the 16*d* site by Co/Hf, we created a structural model with a random distribution of Co and Hf over this site.

This analysis indicates that the electron clouds of Co and Hf atoms strongly overlap with chalcogen atoms highlighting the existence of strong covalent bonding between δ(Co – S) and δ(Hf – S). In this pair of bonds, δ(Co – S) shows slightly stronger overlapping of electron clouds than δ(Hf – S) in $Cu_2CoHf_3S_8$. The overlapping of electron clouds between δ(Co – S) and δ(Hf – S) is much stronger in $Cu_2CoHf_3S_8$ compared to $CuCo_2S_4$ [51] and $CuHf_2S_4$ (Fig. 6 a-c). On the other hand, the weaker overlapping of electron clouds between Cu and S atoms reveals a more ionic nature of chemical bonding between them. Such bonding inhomogeneity between the covalent δ(Co – S) and δ(Hf – S) from one side, and more ionic δ(Cu – S) interactions leads to low lattice thermal conductivity in $Cu_2MeHf_3S_8$ (*Me* – Mn, Fe, Co, Ni) materials.

Moreover, even if the bonding inhomogeneity is present in the $CuCo_2S_4$ structure, this material shows quite high values of sound velocity (v_l = 4377 m s^{-1}, v_t = 2367 m s^{-1}) which leads also to relatively high lattice

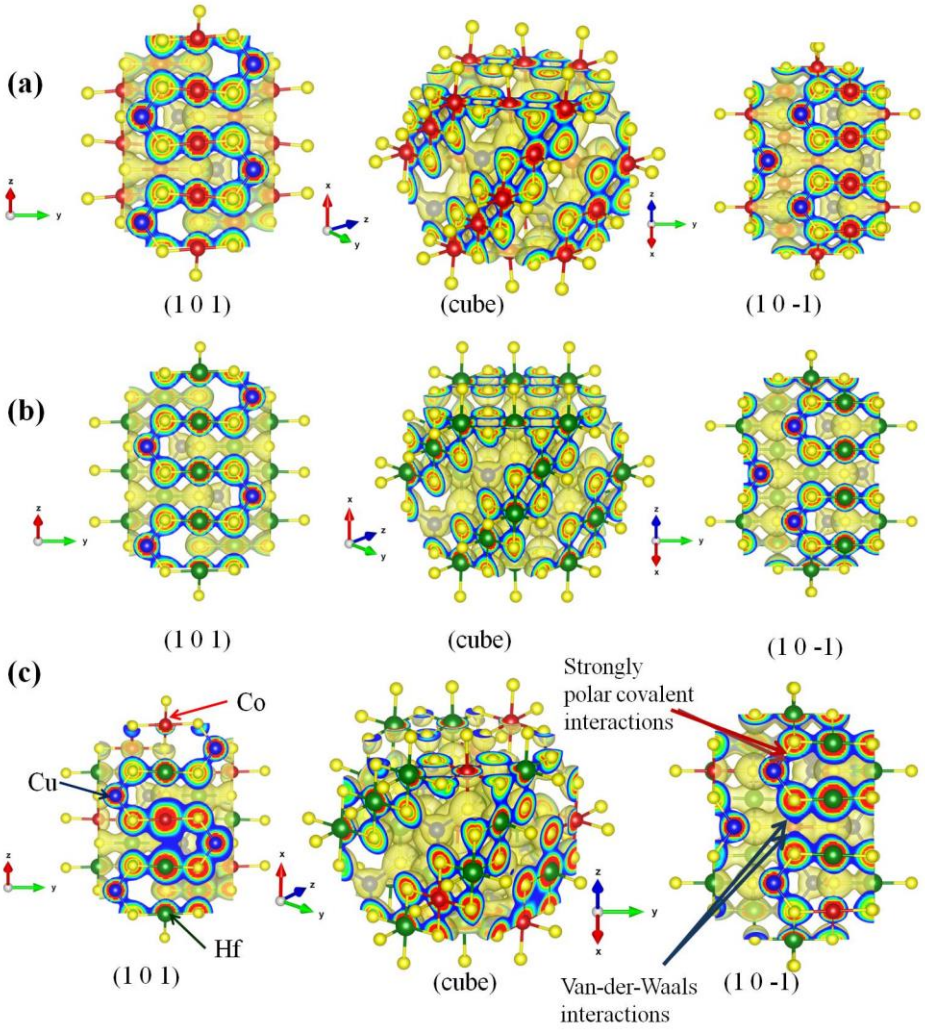

Fig.6. Bonding analysis in $Cu_2CoHf_3S_8$ (a), $CuCo_2S_4$ (b), and $CuHf_2S_4$ (c) by means of electron localization function (ELF) with isosurface value of 0.02 e bohr^{-3} sliced on the planes [1 0 1] and [1 0 -1], respectively.

thermal conductivity in this material (ranging from 1.48 W m^{-1}K^{-1} at 323 K to 0.57 W m^{-1}K^{-1} at 723 K) [51]. Interestingly, strong bonding inhomogeneity observed in $Cu_2CoHf_3S_8$ leads to the lowering of its sound velocity (v_l= 4072 m s^{-1}, v_t = 2172 m s^{-1}) as was hypothesized by Grin [22], this fact causes a significant lowering of lattice thermal conductivity in the material (ranging from 0.78 W m^{-1}K^{-1} at 298 K to 0.50 W m^{-1}K^{-1} at 673 K). This work confirms that bonding inhomogeneity can be effectively used to disturb thermal transport in functional materials.

Conclusions

The analysis of the crystal structure of $Cu_2MeHf_3S_8$ (*Me* – Mn, Fe, Co, Ni) sulfides indicates that if the 16*d* site in spinel structures is occupied by a *d*-element, then the number of electrons in the *d*-sublevel is important. Additionally, the formation of a statistical mixture in this site has an important effect on the electronic properties. Specifically, it was established that the best electronic transport is observed in the presence of the same two valence *d* electrons in both [1Ni:3Hf] atoms. Moreover, random occupation of the 16*d* site by *Me*/Hf atoms in $Cu_2MeHf_3S_8$ (*Me* – Mn, Fe, Co, Ni) leads to a strong bonding inhomogeneity and one of the lowest lattice thermal conductivity in materials with spinel structure type. The best thermoelectric performance of $Cu_2NiHf_3S_8$ can be explained by its highest weighted mobility described by electron scattering on phonons and the low lattice thermal conductivity due to strong bonding inhomogeneity.

Smitiukh Oleksandr – Candidate of Chemical Sciences, Senior Laboratory Technician of the Department of Chemistry and Technologies;
Soroka Oksana **–** Ph.D, Associate Professor of the Department of Forensic Medicine, Medical and Pharmaceutical Law;
Marchuk Oleg – Candidate of Chemical Sciences, Associate Professor of the Department of Chemistry and Technologies.

[1] Z. Chen, X. Zhang, Y. Pei, *Manipulation of Phonon Transport in Thermoelectrics*, Adv. Mater., 30, 1705617 (2018); https://doi.org/10.1002/adma.201705617.
[2] K. Zhao, P. Qiu, X. Shi, L. Chen, *Recent Advances in Liquid-Like Thermoelectric Materials*, Adv. Funct. Mater., 30, 1903867 (2020); https://doi.org/10.1002/adfm.201903867.
[3] T. Ghosh, M. Dutta, D. Sarkar, K. Biswas, I*nsights into Low Thermal Conductivity in Inorganic Materials for Thermoelectrics*, J. Am. Chem. Soc., 144, 10099 (2022); https://doi.org/10.1021/JACS.2C02017/ASSET/IMAGES/LARGE/JA2C02017_0008.JPEG.
[4] R.A. Miller, *Thermal barrier coatings for aircraft engines: History and directions*, J. Therm. Spray Technol., 6, 35 (1997); https://doi.org/10.1007/BF02646310/METRICS.
[5] O. Cherniushok, R. Cardoso-Gil, T. Parashchuk, R. Knura, Y. Grin, K.T. Wojciechowski, *Lone-Pair-Like Interaction and Bonding Inhomogeneity Induce Ultralow Lattice Thermal Conductivity in Filled β-Manganese-Type Phases*, Chem. Mater. 34, 6389 (2022); https://doi.org/10.1021/acs.chemmater.2c00915.
[6] T. Parashchuk, A. Shabaldin, O. Cherniushok, P. Konstantinov, I. Horichok, A. Burkov, Z. Dashevsky, *Origins of the enhanced thermoelectric performance for p-type Ge1-xPbxTe alloys*, Phys. B Condens. Matter. 596, 412397(2020); https://doi.org/10.1016/J.PHYSB.2020.412397.
[7] T. Parashchuk, B. Wiendlocha, O. Cherniushok, R. Knura, K.T. Wojciechowski, *High Thermoelectric Performance of p-Type PbTe Enabled by the Synergy of Resonance Scattering and Lattice Softening*, ACS Appl. Mater. Interfaces, 13, 49027 (2021); https://doi.org/10.1021/acsami.1c14236.
[8] T. Parashchuk, R. Knura, O. Cherniushok, K.T. Wojciechowski, *Ultralow Lattice Thermal Conductivity and Improved Thermoelectric Performance in Cl-Doped Bi2Te3–xSex Alloys*, ACS Appl. Mater. Interfaces. 14, 33567 (2022); https://doi.org/10.1021/acsami.2c08686.
[9] O. Cherniushok, O. V. Smitiukh, J. Tobola, R. Knura, O. V. Marchuk, T. Parashchuk, K.T. Wojciechowski, *Crystal Structure and Thermoelectric Properties of Novel Quaternary Cu2MHf3S8(M-Mn, Fe, Co, and Ni) Thiospinels with Low Thermal Conductivity*, Chem. Mater. 34, 2146 (2022); https://doi.org/10.1021/acs.chemmater.1c03593.
[10] M. Maksymuk, K. Zazakowny, A. Lis, A. Kosonowski, T. Parashchuk, K.T. Wojciechowski, *Development of the anodized aluminum substrates for thermoelectric energy converters*, Ceram. Int. 49, 4816(2023); https://doi.org/10.1016/J.CERAMINT.2022.09.371.
[11] W.G. Zeier, A. Zevalkink, Z.M. Gibbs, G. Hautier, M.G. Kanatzidis, G.J. Snyder, *Thinking Like a Chemist: Intuition in Thermoelectric Materials*, Angew. Chemie Int. Ed. 55, 6826 (2016); https://doi.org/10.1002/ANIE.201508381.
[12] O. Cherniushok, T. Parashchuk, J. Tobola, S.D.N. Luu, A. Pogodin, O. Kokhan, I. Studenyak, I. Barchiy, M. Piasecki, K.T. Wojciechowski, *Entropy-Induced Multivalley Band Structures Improve Thermoelectric Performance in p-Cu7P(SxSe1- x)6Argyrodites*, ACS Appl. Mater. Interfaces., 13, 39606 (2021); https://doi.org/10.1021/acsami.1c11193.
[13] K. Zazakowny, A. Kosonowski, A. Lis, O. Cherniushok, T. Parashchuk, J. Tobola, K.T. Wojciechowski, *Phase Analysis and Thermoelectric Properties of Cu-Rich Tetrahedrite Prepared by Solvothermal Synthesis*, Materials (Basel)., 15, 849(2022); https://doi.org/10.3390/MA15030849.
[14] J. Yang, Y. Wang, H. Yang, W. Tang, J. Yang, L. Chen, W. Zhang, *Thermal transport in thermoelectric materials with chemical bond hierarchy*, J. Phys. Condens. Matter., 31, 183002 (2019); https://doi.org/10.1088/1361-648X/AB03B6.
[15] F. Kateusz, T. Korzec, M. Zambrzycki, O. Cherniushok, M. Gubernat, *Influence of montmorillonite nanoparticles on thermal and mechanical properties of carbon-carbon hybrid composites based on phenolic-formaldehyde resin*, Compos. Theory Pract., 2021, 96 (2021).
[16] H. Liu, X. Shi, F. Xu, L. Zhang, W. Zhang, L. Chen, Q. Li, C. Uher, T. Day, G. Snyder Jeffrey, *Copper ion liquid-like thermoelectrics*, Nat. Mater., 11, 422 (2012); https://doi.org/10.1038/nmat3273.
[17] L.D. Zhao, S.H. Lo, Y. Zhang, H. Sun, G. Tan, C. Uher, C. Wolverton, V.P. Dravid, M.G. Kanatzidis, *Ultralow thermal conductivity and high thermoelectric figure of merit in SnSe crystals*, Nature., 508, 373 (2014); https://doi.org/10.1038/nature13184.
[18] X.L. Shi, J. Zou, Z.G. Chen, *Advanced Thermoelectric Design: From Materials and Structures to Devices*, Chem. Rev., 120, 7399 (2020); https://doi.org/10.1021/acs.chemrev.0c00026.
[19] E.J. Skoug, D.T. Morelli, *Role of lone-pair electrons in producing minimum thermal conductivity in nitrogen-group chalcogenide compounds*, Phys. Rev. Lett., 107, 235901(2011); https://doi.org/10.1103/PHYSREVLETT.107.235901/FIGURES/4/MEDIUM.
[20] C. Chang, L.D. Zhao, *Anharmoncity and low thermal conductivity in thermoelectrics*, Mater. Today Phys., 4, 50 (2018); https://doi.org/10.1016/J.MTPHYS.2018.02.005.
[21] O. V. Smitiukh, O. V. Marchuk, Y.M. Kogut, V.O. Yukhymchuk, N. V. Mazur, G.L. Myronchuk, S.M. Ponedelnyk, O.I. Cherniushok, T.O. Parashchuk, O.Y. Khyzhun, T. Wojciechowski, A.O. Fedorchuk, *Effect of rare-earth doping on the structural and optical properties of the Ag3AsS3 crystals*, Opt. Quantum Electron., 54, (2022); https://doi.org/10.1007/S11082-022-03542-W.
[22] Y. Grin, *Inhomogeneity and anisotropy of chemical bonding and thermoelectric properties of materials*, J. Solid State Chem., 274, 329 (2019); https://doi.org/10.1016/J.JSSC.2018.12.055.

[23] A. Ormeci, Y. Grin, *Coexistence of ionic and covalent atomic interactions (bonding inhomogeneity) and thermoelectric properties of intermetallic clathrates*, J. Thermoelectr., 6, 16 (2015).
[24] M. Dutta, K. Pal, U. V. Waghmare, K. Biswas, *Bonding heterogeneity and lone pair induced anharmonicity resulted in ultralow thermal conductivity and promising thermoelectric properties in n-type AgPbBiSe3*, Chem. Sci., 10, 4905(2019); https://doi.org/10.1039/C9SC00485H.
[25] F. Huiying, *Environmentally friendly and earth-abundant colloidal chalcogenide nanocrystals for photovoltaic applications*, J. Mater. Chem. C., 6, 414 (2018).
[26] F.T. Farheen F.Jaldurgam, Zubair Ahmad, *Low-Toxic, Earth-Abundant Nanostructured Materials for Thermoelectric Applications*, Nanomaterials. 11, 895 (2021); https://doi.org/10.3390/nano11040895.
[27] M.R. Huch, L.D. Gulay, I.D. Olekseyuk, *Crystal structures of the R3Mg0.5GeS7 (R = Y, Ce, Pr, Nd, Sm, Gd, Tb, Dy, Ho and Er) compounds*, J. Alloys Compd., 424, 114 (2006); https://doi.org/10.1016/j.jallcom.2005.12.025.
[28] L.D. Gulay, M. Daszkiewicz, M.R. Huch, A. Pietraszko, *Ce3Mg0.5GeS7 from single-crystal data*, Acta Crystallogr. Sect. E Struct. Reports Online. 63 (2007); https://doi.org/10.1107/S1600536807048593.
[29] Y. He, T. Day, T. Zhang, H. Liu, X. Shi, L. Chen, G.J. Snyder, *High thermoelectric performance in non-toxic earth-abundant copper sulfide*, Adv. Mater., 26, 3974 (2014); https://doi.org/10.1002/adma.201400515.
[30] R. Ang, A.U. Khan, N. Tsujii, K. Takai, R. Nakamura, T. Mori, *Thermoelectricity Generation and Electron-Magnon Scattering in a Natural Chalcopyrite Mineral from a Deep-Sea Hydrothermal Vent*, Angew. Chemie - Int. Ed. 54, 12909 (2015); https://doi.org/10.1002/anie.201505517.
[31] Y. Kim, S.-W. Kang, H.-U. Kim, al -, N. Kryzhanovskaya, A. Zhukov, E. Moiseev, D. Zhang, H.-C. Bai, Z.-L. Li, J.-L. Wang, G.-S. Fu, S.-F. Wang, *Multinary diamond-like chalcogenides for promising thermoelectric application**, Chinese Phys. B., 27, 047206 (2018); https://doi.org/10.1088/1674-1056/27/4/047206.
[32] S. Fiechter, M. Martinez, G. Schmidt, W. Henrion, Y. Tomm, *Phase relations and optical properties of semiconducting ternary sulfides in the system Cu–Sn–S*, J. Phys. Chem. Solids., 64,) 1859 (2003); https://doi.org/10.1016/S0022-3697(03)00172-0.
[33] V. Pavan Kumar, P. Lemoine, V. Carnevali, G. Guélou, O.I. Lebedev, P. Boullay, B. Raveau, R. Al Rahal Al Orabi, M. Fornari, C. Prestipino, D. Menut, C. Candolfi, B. Malaman, J. Juraszek, E. Guilmeau, *Ordered sphalerite derivative Cu5Sn2S7: a degenerate semiconductor with high carrier mobility in the Cu–Sn–S diagram*, J. Mater. Chem. A., 9, 10812 (2021); https://doi.org/10.1039/D1TA01615F.
[34] C. Bourgès, Y. Bouyrie, A.R. Supka, R. Al Rahal Al Orabi, P. Lemoine, O.I. Lebedev, M. Ohta, K. Suekuni, V. Nassif, V. Hardy, R. Daou, Y. Miyazaki, M. Fornari, E. Guilmeau, *High-Performance Thermoelectric Bulk Colusite by Process Controlled Structural Disordering*, J. Am. Chem. Soc., 140, 2186 (2018); https://doi.org/10.1021/jacs.7b11224.
[35] R. Chetty, A. Bali, R.C. Mallik, T*etrahedrites as thermoelectric materials: An overview*, J. Mater. Chem. C., 3, 12364 (2015); https://doi.org/10.1039/c5tc02537k.
[36] S. Lin, W. Li, Y. Pei, *Thermally insulative thermoelectric argyrodites*, Mater. Today., 48, 198(2021); https://doi.org/10.1016/J.MATTOD.2021.01.007.
[37] P. Lemoine, G. Guélou, B. Raveau, E. Guilmeau, *Crystal Structure Classification of Copper-Based Sulfides as a Tool for the Design of Inorganic Functional Materials*, Angew. Chemie Int. Ed., 61, e202108686 (2022); https://doi.org/10.1002/ANIE.202108686.
[38] X. Shen, C.C. Yang, Y. Liu, G. Wang, H. Tan, Y.H. Tung, G. Wang, X. Lu, J. He, X. Zhou, *High-Temperature Structural and Thermoelectric Study of Argyrodite Ag 8 GeSe 6*, ACS Appl. Mater. Interfaces. 11, 2168 (2019); https://doi.org/10.1021/acsami.8b19819.
[39] F. Baumer, T. Nilges, *Phase Segregation of Polymorphic Solid Ion Conducting Cu7PSe6 during Thermoelectric Experiments*, Zeitschrift Für Anorg. Und Allg. Chemie. 644, 1519(2018); https://doi.org/10.1002/ZAAC.201800108.
[40] G. Strick, G. Eulenberger, H. Hahn, *Über einige quaternäre Chalkogenide mit Spinellstruktur*, ZAAC - J. Inorg. Gen. Chem. 357, 338 (1968); https://doi.org/10.1002/zaac.19683570421.
[41] J.J. Snyder, T. Caillat, J.P. Fleurial, *Thermoelectric properties of chalcogenides with the spinel structure*, Mater. Res. Innov., 5, 67 (2001); https://doi.org/10.1007/s100190100133.
[42] L. Akselrud, Y. Grin, *WinCSD: Software package for crystallographic calculations (Version 4)*, J. Appl. Crystallogr., 47, 803 (2014); https://doi.org/10.1107/S1600576714001058.
[43] K. Momma, F. Izumi, *VESTA 3 for three-dimensional visualization of crystal, volumetric and morphology data*, J. Appl. Crystallogr., 44, 1272 (2011); https://doi.org/10.1107/S0021889811038970/FULL.
[44] The PC GAMESS/Firefly - REFERENCE, (n.d.).
[45] G.M.J. Barca, C. Bertoni, L. Carrington, D. Datta, N. De Silva, J.E. Deustua, D.G. Fedorov, J.R. Gour, A.O. Gunina, E. Guidez, T. Harville, S. Irle, J. Ivanic, K. Kowalski, S.S. Leang, H. Li, W. Li, J.J. Lutz, I. Magoulas, J. Mato, V. Mironov, H. Nakata, B.Q. Pham, P. Piecuch, D. Poole, S.R. Pruitt, A.P. Rendell, L.B. Roskop, K. Ruedenberg, T. Sattasathuchana, M.W. Schmidt, J. Shen, L. Slipchenko, M. Sosonkina, V. Sundriyal, A. Tiwari, J.L. Galvez Vallejo, B. Westheimer, M. Włoch, P. Xu, F. Zahariev, M.S. Gordon, *Recent developments in the general atomic and molecular electronic structure system*, J. Chem. Phys. 152, 154102 (2020); https://doi.org/10.1063/5.0005188.

[46] I. V. Horichok, L.I. Nykyruy, T.O. Parashchuk, S.D. Bardashevska, M.P. Pylyponuk, *Thermodynamics of defect subsystem in zinc telluride crystals*, Mod. Phys. Lett. B., 30, (2016); https://doi.org/10.1142/S0217984916501724.
[47] D. Freik, T. Parashchuk, B. Volochanska, *Thermodynamic parameters of CdTe crystals in the cubic phase*, J. Cryst. Growth., 402, 90 (2014); https://doi.org/10.1016/J.JCRYSGRO.2014.05.005.
[48] Chemcraft - Graphical program for visualization of quantum chemistry computations, (n.d.).
[49] G.J. Snyder, A.H. Snyder, M. Wood, R. Gurunathan, B.H. Snyder, C. Niu, *Weighted Mobility*, Adv. Mater. 32, 2001537 (2020); https://doi.org/10.1002/ADMA.202001537.
[50] T. Parashchuk, I. Horichok, A. Kosonowski, O. Cherniushok, P. Wyzga, G. Cempura, A. Kruk, K.T. Wojciechowski, *Insight into the transport properties and enhanced thermoelectric performance of n-type Pb1−xSbxTe*, J. Alloys Compd., 860, 158355 (2021); https://doi.org/10.1016/J.JALLCOM.2020.158355.
[51] Y. Lang, L. Pan, C. Chen, Y. Wang, *Thermoelectric Properties of Thiospinel-Type CuCo2S4*, J. Electron. Mater. 48, 4179 (2019); https://doi.org/10.1007/s11664-019-07182-x.

Олександр Смітюх[1], Оксана Сорока[2], Олег Марчук[1]

Вплив кристалічної структури та хімічних зв'язків на електронні та теплові властивості у шпінелях $Cu_2MeHf_3S_8$ (Me – Mn, Fe, Co, Ni)

[1]*Факультет хімії, екології та фармації, Волинський національний університет імені Лесі Українки, м. Луцьк, Україна, Smitiukh.Oleksandr@vnu.edu.ua*
[2]*Івано-Франківський національний медичний університет, Івано-Франківськ, Україна*

Встановлення взаємозв'язків між кристалічною структурою та транспортними властивостями є важливою проблемою, що безпосередньо пов'язана із застосуванням функціональних матеріалів. У цій роботі нами представлено аналіз кристалічної структури, хімічних зв'язків, електронних та теплових транспортних властивостей сполук $Cu_2MeHf_3S_8$ (*Me* – Mn, Fe, Co, Ni). Збільшення рухливості носіїв заряду в ряду Mn → Fe → Co → Ni, а також зміна домінуючого механізму розсіювання носіїв заряду від росіювання на точкових дефектах до розсіювання на акустичних фононах пояснює найкращий рух електронів у сполуці $Cu_2NiHf_3S_8$. Окрім цього, неоднорідність зв'язків між ковалентним для δ(Co – S) і δ(Hf – S) з одного боку та більш іонним для δ(Cu – S) з іншої сторони призводить до низької теплопровідності в матеріалах $Cu_2MeHf_3S_8$ (*Me* – Mn, Fe, Co, Ni). У роботі також пропонується оглях зв'язку між зайнятістю октедричної 16*d* ПСТ і термоелектричними параметрами досліджених тіошпінелей. Варто зазначити, що найкращі термоелектричні параметри спостерігаються у тому випадку, коли в суміші присутні два валентних електрони на *d*-підрівні атомів, що займають октаедричні позиції, що може бути важливим для подальших досліджень з метою покращення термоелектричних параметрів тіошпінелей.

Ключові слова: неоднорідність зв'язків; кристалічна структура; рухливість носіїв заряду; теплопровідність; тетрарні сульфіди.